Model-based Measurement of Particle Size Distributions in Layering Granulation Processes

Andreas Bück, Mirko Peglow, and Evangelos Tsotsas
Chair of Thermal Process Engineering, Otto-von-Guericke University, Universitätsplatz 2, 39106 Magdeburg, Germany

Michael Mangold
Max-Planck-Institut für Dynamik komplexer technischer Systeme, Sandtorstraße 1, 39016 Magdeburg, Germany

Achim Kienle
Chair of Automation/Modeling, Otto-von-Guericke University, Universitätsplatz 2, 39106 Magdeburg, Germany

DOI 10.1002/aic.12314
Published online June 17, 2010 in Wiley Online Library (wileyonlinelibrary.com).

In this work, we present a method for the online estimation of particle size distributions in layering granulation processes using a methodology known as model-based measurement or state estimation. After presenting the necessary model equations for two practically relevant processes it is investigated which quantities of the processes have to be measured to estimate the size distribution. For the different processes square-root unscented Kalman filters (SR-UKF) are designed and tested in simulations to demonstrate the feasibility of this approach. © 2010 American Institute of Chemical Engineers *AIChE J,* 57: 929–941, 2011

Keywords: process systems engineering, state estimation, population balance models, granulation, fluidized bed

Introduction

In many particulate processes, the particle size distribution is of paramount interest to assess the process success and the necessary downstream processing of the product (e.g., separation or drying). Industrial requirements, for example from food and pharmaceutical industries, give rise to the need to influence the particle size distribution directly, for example, by feedback control. Modern feedback control methodologies often require the knowledge of the current ''state'' of the process under consideration — in case of particulate processes this includes the particle size distribution.

Currently there are few measurement systems available that allow the online measurement of chord length distributions, for example, the FBRM probe by Lasentec or the IPP-70 by Parsum GmbH. Using fibre-optical methods and a geometric model for the particles a chord length is determined for each particle that enters the measurement volume. In applications this approach faces at least two severe problems: First is the measurement of particles (or agglomerates) that do not fit into the geometric model, second is the determination of a particle size distribution from the obtained chord length distribution. While, a partial solution to the former problem requires extensive process-specific calibration of the probe, the latter states a highly ill-conditioned problem of inverting the measurement map because of the corruption of the measurements by noise. In case of the often applied FBRM probe Kail et al.[1] proposed an inversion method that utilizes an optical model of the lenses in the probe.

Correspondence concerning this article should be addressed to A. Bück at andreas.bueck@ovgu.de.

Additionally, detailed mathematical models — mostly based on the population balance approach introduced by Hulburt and Katz[2] and brought to a wide audience by the work of Ramkrishna[3] — for the analysis of the dynamical behavior have emerged and experimentally validated. This leads to the question why not to use this mathematical process models to gain additional process information from (more easily obtainable) online measurements?

One possible approach is the use of model-based measurement methods, also known as state observation or state estimation techniques. They allow — under certain conditions — the online reconstruction of not directly measurable quantities from directly measurable noisy quantities. The concept was introduced by the works of Kalman[4] and Luenberger[5] in the 1960s–1970s for linear systems and extended to nonlinear systems in the following decades.[6–10]

In the area of chemical process engineering several successful applications of state estimation schemes are available, see for example Zeitz,[11] Aguilar-López and Maya-Yescas,[12] Bastin and Dochain,[13] and Mangold et al.[14]

We will apply one particular method — the square-root unscented Kalman filter — to two practically relevant granulation processes: a batch granulation process and a continuous granulation with external classification and particle reflux. In this first of two parts, we will present the theoretical considerations that come with the setup of a model-based measurement system, in the second part, we will present the experimental results obtained using the method presented here.

In this work, we will concentrate on the determination of suitable measurements (by means of a structural observability analysis) and the design of a suitable square-root unscented Kalman filter, SRUKF for short. In doing so, we will point out some practical guidelines for the setup of the SRUKF.

This article is structured as follows: After a short overview on the principles of model-based measurement the two example processes are described and their mathematical models are summarized. Then the SRUKF methodology is described and for both processes an estimator is designed. This work concludes with a presentation and discussion of the simulation results with respect to measurement and model uncertainties as well as real-time constraints.

Principles of Model-based Measurement

The general structure of a model-based measurement scheme can be summarised as follows: A dynamical process model (in the form of mathematical equations) is simulated in parallel to the real existing plant. Inputs to the plant are fed identically to the simulation model, and (suitably chosen) measurements obtained from the plant are also calculated from the state information of the simulation model. In the absence of model errors, exogeneous disturbances and identical initial conditions of the plant and the simulation model, this configuration is able to reconstruct the state information of the plant from the available plant measurements. However, the initial conditions are almost never exactly known and model errors or exogeneous disturbances are in most processes inevitable. Using the configuration just described would lead to erroneous results.

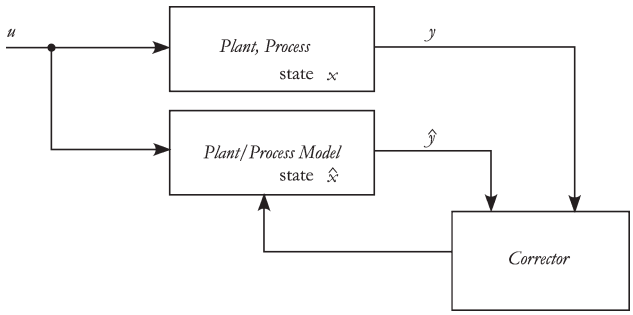

Figure 1. Observer structure as introduced by Luenberger; u denotes the inputs to the systems, y is the plant measurement, ŷ is the observer measurement.

Augmenting the configuration by a correction term that depends solely on the plant measurements, the simulated measurements from the mathematical model, and the system inputs results in the so called Luenberger structure of a state observer, see Figure 1. If a system is observable (under a certain set of measured quantities) then the correction term can be designed such that if the difference in the measurements tends to zero the state of the simulation model converges to the (unmeasurable) state of the plant.

In the following, we will call a system observable if it complies to the following

Definition. A dynamical system in state-space representation

$$x'(t) = f(x(t), u(t)), \tag{1}$$

$$y(t) = h(x(t), u(t)), \tag{2}$$

where $x \in \mathbb{R}^N$ denotes the state of the system, $u \in \mathbb{R}^U$ are the inputs to the system, and $y \in \mathbb{R}^M$ represent the measurement information, is said to be observable if the state $x(\theta)$ at a given time θ is completely determined by the knowledge of the inputs $u(\tau)$ and the outputs $y(\tau)$ over a finite time segment $t_0 < \tau \leq \theta$.[15] For general nonlinear systems, this is only true for a certain set of initial conditions x_0 and inputs $u(t)$. These systems are called locally observable.[16]

The test whether a given set of measurements is suitable for state estimation purposes or the determination of quantities which have to be measured in order to reconstruct the state profiles is called observability analysis.

As the algebraic criteria for observability[17] of high-dimensional nonlinear systems are very hard to verify, we limit ourselves to a structural observability analysis[18,19] based on the linearisation of the process model.

If a system is structurally observable then there exists an observable system with the same structure. Although the test does not provide specific information about the system at hand, it tells that it is not unobservable and therefore a state estimator can be designed.

The actual design process depends on the methodology used. The design of the estimator chosen for this work will be described in detail in a subsequent section.

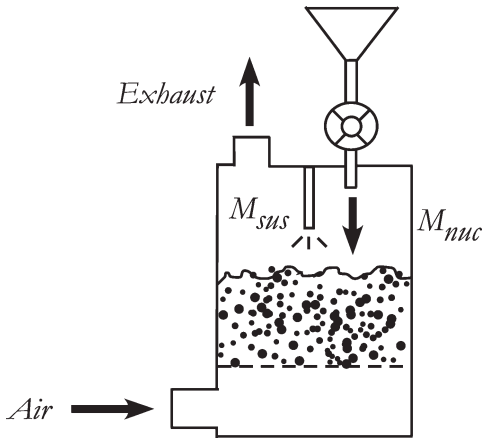

Figure 2. Simplified schematic of a batch spray granulator.

Process Description

This section is a summary of the description and mathematical modelling of the two particulate processes under consideration: first is a fluidized bed batch spray granulation, the second is a continuous spray granulation process with external classification and particle reflux as investigated by Heinrich et al.[20] and Radichkov et al.,[21] amongst others. Although, the first process gives the possibility for comparison with state estimation schemes in other particulate processes (e.g., crystallisation[14]), the second application serves two purposes: (1) to show the generality in use of the chosen state estimation scheme and (2) to provide the first application of model-based measurement to a continuous granulation process with particle reflux.

Fluidized bed spray granulation

Fluidized bed spray granulation is used to create dustless free-flowing powders from a liquid suspension. This suspension is sprayed on small particles and (externally supplied) nuclei inside the apparatus. Drying of the suspension on the particle surface then leads to a growth of the particles. The most interesting property for this granulation process is the particle size ξ of the particles. In the following, it is assumed that the dominating particulate process is the growth in particle size because of layer formation on the surface, that is, aggregation and breakage phenomena are neglected. The influence of these phenomena can be limited by suitably chosen operating conditions, see Ennis et al.[22]

The suspension is fluidized by air and kept in a well-mixed state. In a batch configuration a certain initial distribution of particles and a certain flux of nuclei is supplied. A simplified schematic of this process can be seen in Figure 2.

Under the assumptions of a well-mixed system, a population balance approach leads to a population balance equation for the time-varying particle size distribution density $n(t,\xi)$:

$$\frac{\partial n}{\partial t} = -\frac{\partial (Gn)}{\partial \xi}. \tag{3}$$

In this equation, G describes the growth of the particles because of the spraying of a suspension with density ϱ_s and a mass flow rate M_{sus}. Under the assumption of surface-proportional growth of spherical particles,[23] G can be described by

$$G(t,n) = 2\,\frac{M_{\text{sus}}}{\varrho_s A_{\text{bed}}(t,n)}, \tag{4}$$

$$A_{\text{bed}}(t,n) = \pi \int_0^\infty \xi^2 n(t,\xi)\,\mathrm{d}\xi. \tag{5}$$

As can be seen the growth rate is size-independent. Because of the nonlinearity of G (with respect to n) the population balance equation is nonlinear. Additionally, initial and boundary conditions have to be specified, for example,

$$n(t_0,\xi) = \psi(\xi), \tag{6}$$

$$G(t,n)n(t,\xi_0) = j_{\text{nuc}}(t, M_{\text{nuc}}). \tag{7}$$

The quantity j_{nuc} describes the flux of nuclei that enters the system with a mass flow rate M_{nuc}. The flow rates M_{sus} and M_{nuc} can be considered as inputs to the batch granulator (e.g., for control purposes).

The general behavior is qualitativly given by a nonlinear transport of the initial particle size distribution density $n(t_0,\xi)$ along the property coordinate ξ, as seen in Figure 3. For a detailed analysis of the behaviour of such nonlinear transport systems, see for instance Evans.[24]

Continuous fluidized bed granulation with external classification

The continuous process consists of a spray granulator as described above but with a continuous external feed and outlet of particles. The outlet flux is screened: The oversized particles from the first screen are milled to a size ξ_M and refed into the granulator, the undersized particles are screened once more. Here, the oversized particles are kept as product, whereas the undersized particles are also refed into

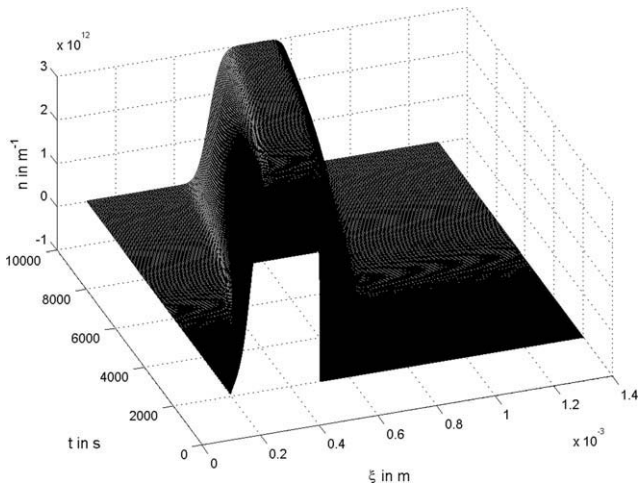

Figure 3. Qualitative behavior of the particle size distribution density in a batch spray granulation process.

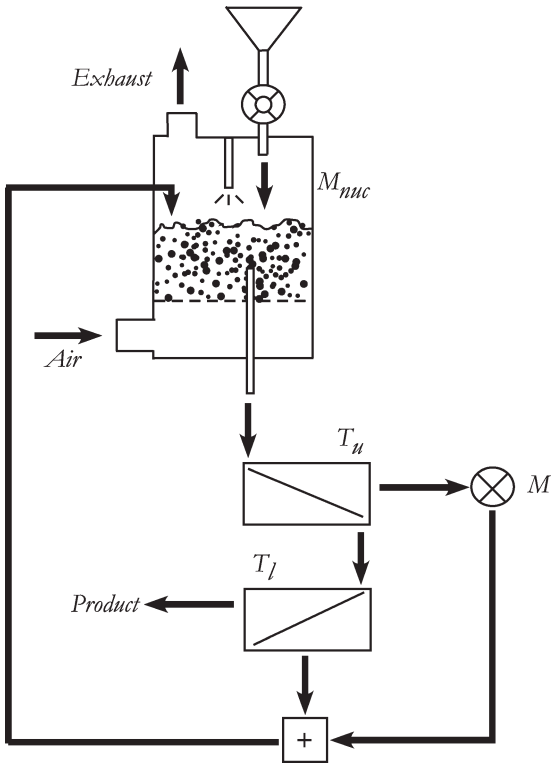

Figure 4. Flowsheet of a continuous spray granulation with external classification.

the granulator for further growth. A flowsheet of this process is depicted in Figure 4.

This process system was extensively investigated by Heinrich et al.[20] and Radichkov et al.[21] concerning the dynamic behaviour. A population balance equation for the particle size distribution density — under the assumptions of well-mixedness, and spherical particles with the property coordinate ξ — reads

$$\frac{\partial n}{\partial t} = -\frac{\partial (Gn)}{\partial \xi} + [(1 - T_l)(1 - T_u) - 1]Kn + M\delta(\xi - \xi_M), \tag{8}$$

where K is an outlet kinetics (controlled for a constant bed mass) and T is a sieving operator and M is the milling operator for the mill. They are given, respectively, by the following equations:

$$K = 1 - \min(1, m_{\text{bed}}(t_0)/m_{\text{bed}}(t)), \tag{9}$$

$$T_{l/u}(\xi) = \begin{cases} 0, & \xi \le \xi_{l/u} \\ 1, & \xi > \xi_{l/u} \end{cases}, \tag{10}$$

$$M = \frac{M_{\text{nuc}}}{m_{\text{nuc}}}. \tag{11}$$

The growth kinetics is again given by Eqs. 4–5. As was shown in Radichkov et al.[21] the process exhibits different dynamic behavior depending on the value of the milling diameter ξ_M: For a certain range a steady-state distribution is attained, but for a large parameter range the system exhibits sustained oscillations in the particle size distribution density. Typical examples for both regimes are shown in Figures 5 and 6.

Design of a State Estimator for the Particle Size Distribution Density

The task of designing a state estimator consists of two steps: At first a suitable set of measurements has to be determined, and second the estimator itself has to be calculated following the necessary steps of the methodology chosen.

We will show in the next subsection — by structural observability analysis — that in both processes any measurement of a (normalized) moment of the size distribution density satisfies the necessary conditions for observability. Using one specific measurement, the average particle size, a square-root unscented Kalman filter is designed for the dynamic reconstruction of the particle size distribution density from this scalar measurement.

To use the concepts introduced earlier, the model equations of both processes, described by partial differential equations, have to be put into the finite dimensional state-space framework. For this the partial derivatives with respect to the property coordinate are approximated, for example, by a first-order finite volume method using an upwind scheme for the convective parts of the model. The integral for the bed surface A_{bed} is also approximated. Here, a composite tangent trapezium rule is used.

The model equations can then be written as

$$\frac{\mathrm{d}\mathbf{n}}{\mathrm{d}t} = -G\mathcal{D}_N\mathbf{n} + \mathbf{f}(\mathbf{n}) + \mathbf{g}(\mathbf{n})u, \tag{12}$$

$$G = 2\,\frac{\boldsymbol{M}_{sus}}{\varrho_s \pi \langle \mathbf{w}_2, \mathbf{n} \rangle}, \tag{13}$$

which is of the desired form. Here the (regular) matrix $\mathcal{D}_N \in \mathbb{R}^{N\times N}$ is a finite dimensional approximation of the derivative operator $\partial/\partial\xi$. The integral approximation $\langle \mathbf{w}_2, \mathbf{n} \rangle$ is a short hand for

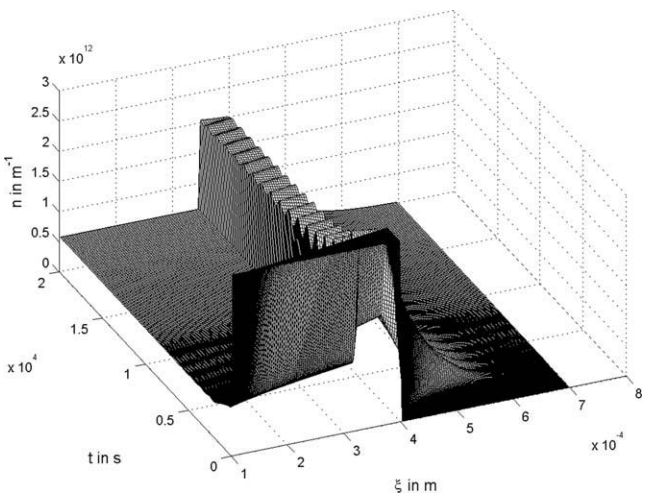

Figure 5. Qualitative behavior of the particle size distribution density in a continuous spray granulation process for a milling diameter ξ_M that leads to a stable steady-state distribution.

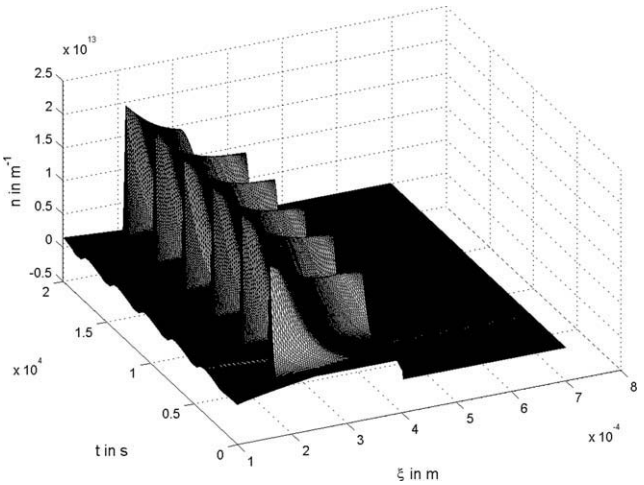

Figure 6. Qualitative behavior of the particle size distribution density in a continuous spray granulation process with a milling diameter that leads to sustained oscillations in the size distribution.

$$\langle \mathbf{w}_2, \mathbf{n} \rangle = \mathbf{w}_2^T \mathbf{n} = \sum_{i=1}^{N} w_{2,i} n(t, \xi_i) = \sum_{i=1}^{N} \xi_i^2 \, n(t, \xi_i) \, \Delta\xi_i \tag{14}$$

using the standard Euclidean scalar product of two finite dimensional vectors. In general, we introduce the notation

$$\langle \mathbf{w}_k, \mathbf{n} \rangle = \mathbf{w}_k^T \mathbf{n} = \sum_{i=1}^{N} \xi_i^k \, n(t, \xi_i) \, \Delta\xi_i \tag{15}$$

for the approximation of the kth moment ($k \geq 0$) of a given distribution density $\mathbf{n}$.

In case of the batch granulation process $\mathbf{f}(\mathbf{n}) \equiv \mathbf{0}$ holds. For the continuous granulation process with external classification it is

$$\mathbf{f}(\mathbf{n}) = [(1 - T_l)(1 - T_u) - 1] K\mathbf{n} + M\delta(\xi - \xi_M), \tag{16}$$

and $\mathbf{g}(\mathbf{n})$ describes the influence of the boundary condition on the $\mathbf{n}_i$ ($i = 1,\ldots,N$).

By choosing a large number of grid nodes for the discretised property coordinate the (pointwise) error between the solution of the original problem, stated as a partial differential equation, and the approximate problem, stated as a system of nonlinear ordinary differential equations, can be made sufficiently small.

Observability Analysis

As was motivated, the actual computation of the observability map for high-dimensional systems is not tractable. Therefore we limit ourselves to a structural observability analysis. We will investigate this observability property for two families of scalar measurements: $y_k = \mu_k$ the kth unnormalized moment of the particle size distribution density, and $\tilde{y}_k = \mu_k/\mu_0$ the normalized or averaged kth moment. Using the introduced notation these measurements can also be expressed as

$$y_k = \langle \mathbf{w}_k, \mathbf{n} \rangle, \quad \tilde{y}_k = \frac{\langle \mathbf{w}_k, \mathbf{n} \rangle}{\langle \mathbf{w}_0, \mathbf{n} \rangle}. \tag{17}$$

In the following, we will treat the observability analysis for both processes and both measurement families simultaneously.

We start with an investigation of the output-connectedness: In case of $y_k = \langle \mathbf{w}_k, \mathbf{n} \rangle$ the measurement is linear with respect to the approximated size distribution $\mathbf{n}$, therefore the structural matrix $C_{s,k}$ (in this case just a row vector) can be obtained by inspection. As all weights $w_{k,i} \neq 0$ it follows $C_{s,k} = [1,\ldots,1]$, that is, all model states have direct influence on the measurement and the process is output-connected. As this property does not depend on the dynamics of the model, it holds for both processes.

In case of $\tilde{y}_k = \langle \mathbf{w}_k, \mathbf{n} \rangle / \langle \mathbf{w}_0, \mathbf{n} \rangle$ — which is nonlinear in $\mathbf{n}$ — at first the linear approximation has to be obtained. A straight-forward computation yields

$$\tilde{y}_k = \frac{1}{\langle \mathbf{w}_0, \mathbf{n} \rangle^2} \left[\mathbf{w}_k^T \langle \mathbf{w}_0, \mathbf{n} \rangle - \langle \mathbf{w}_k, \mathbf{n} \rangle \mathbf{w}_0^T \right] + \text{h.o.t.}. \tag{18}$$

Evaluating the scalar products and simplifying the terms in square brackets shows, under the assumption that $\mathbf{n}$ is not identically zero for all times, that every entry of the row vector is not identically zero. Therefore, the structural matrix $\tilde{C}_{s,k}$ has the form $\tilde{C}_{s,k} = [1, \ldots, 1]$, and output-connectedness for both processes under this family of measurements follows immediately.

Now we will investigate whether the processes under consideration also possess the property of noncontraction.

From Eq. 4 it can be seen that the growth rate G is nonzero for all relevant applications. G vanishes only in case of an infinite bed surface (never attained in practice) or in case of $M_{\text{sus}} = 0$, which is contradictory to the aim of the process.

The linearization of the convective term in Eq. 12 can be obtained by application of the product rule:

$$F = \frac{\partial}{\partial \mathbf{n}} [-(\mathcal{D}_N \mathbf{n}) G] = -\left[\frac{\partial}{\partial \mathbf{n}} (\mathcal{D}_N \mathbf{n}) G + (\mathcal{D}_N \mathbf{n}) \frac{\partial G}{\partial \mathbf{n}} \right]. \tag{19}$$

A similar computation using the definition of the growth rate yields

$$\frac{\partial G}{\partial \mathbf{n}} = -\omega^T G, \tag{20}$$

where the entries of ω are given by $\omega_i = \mathbf{w}_{2,i} / \langle \mathbf{w}_2, \mathbf{n} \rangle \neq 0$.

Using standard results of multivariable calculus this leads to

$$F = -\mathcal{D}_N \left[I_N - \mathbf{n} \, \omega^T \right] G, \tag{21}$$

where I_N denotes the $N \times N$ identity matrix.

From this follows immediately that the structural matrix F_s has a diagonal of ones as a result of the regularity of $\mathcal{D}_N$, in fact — because of the structure of G — it can be shown by evaluation of the expression above that there are no zero entries in the structural matrix. The s-rank of such a square matrix is by definition equal to the number of columns N.

As both processes contain this convective term and the additional term $\mathbf{f}(\mathbf{n})$ of the continuous process does not eradicate nonzero entries from the structural matrix F_s, they are output-connected and noncontracting under the two measurement families, and therefore structurally observable.

Remark: The analysis neither depends on a certain number of grid nodes used in the discretization nor on a special discretization scheme as long as the form (12) is obtained. However, the analysis does not point out which measurements are practically useful as it depends on the sensitivity to changes in the size distribution. This has to be checked additionally, for example, in simulations, or can be inferred from the process conditions.

The Square-Root Unscented Kalman Filter

The square-root unscented Kalman filter (SRUKF) is a descendant of the Kalman filter that allows the estimation of states in linear systems from noisy measurements. The roots of this technique — and its mathematical foundations — can be traced back to the early work of Gauss and Bayes (for a historical overview see Sorenson[25]). Although the Kalman filter provides an optimal estimate of the mean and the variance of the states this is no longer true for nonlinear systems. The extended Kalman filter (EKF), which is often used in industrial applications, uses a linearisation of the nonlinear process to calculate the state correction term and can only give a first order approximation of the variance of the states. In case of highly nonlinear processes that are only poorly described by their linearisations the filter is known to diverge, which makes it unusable for control purposes.

The SRUKF uses a technique known as unscented transform introduced by Julier et al.[26] to gain higher order approximations of the estimates and to reduce the possibility of divergence of the filter because of nonlinear effects.

We will now describe in more detail the general idea behind the SRUKF.

Description

Given a nonlinear time-invariant dynamical system in state space representation

$$x'(t) = f(x,u) + v, \tag{22}$$

$$y_k = h(x_k, u_k) + w_k, \tag{23}$$

where $x \in \mathbb{R}^N$ denotes the state of the system, $y_k \in \mathbb{R}^M$ is the measurement at consecutive times t_k, $(k \geq 0)$, $v \sim N(0,R_v)$ denotes the white process noise with zero mean and spectral density matrix R_v, and the normally distributed measurement noise $w \sim N(0,R_w)$ with zero mean and covariance R_w. It is assumed in the following that v and w are uncorrellated random variables.

Because of the influence of the noise terms v and w on the states these are no longer deterministic but also random variables with a certain mean and (co)variance. The main idea of the unscented transform is to propagate the distribution through the process nonlinearity f and then calculate an approximation of the new mean and covariance. This is in contrast to the EKF, which approximates the nonlinearity and then propagates the mean and covariance by this approximation.

According to the work of Julier and co-workers,[26,27] a state estimate $\hat{x}$ of the unknown state x can be reconstructed by a predictor-corrector approach. We will use the square-root modification of the unscented tranform by van der Merwe and Wan[28] which has better numerical properties:

Initialization. The observer state $\hat{x}_0$ is set to the initially guessed values. From this the matrix square root of the covariance matrix, S_0, is calculated by a Cholesky decomposition:

$$\hat{x}_0 = E\{x_0\}, \quad S_0 = \text{cholesky}(P_0). \tag{24}$$

For the simulations P_0 is calculated by the dyadic product of the differences between model and observer state. To maintain positive definiteness a small multiple of the identity matrix is added.

Prediction. For every measurement time step $k = 1,2,\ldots$ a finite number $(2N + 1)$ of sigma points (points in state space that capture the mean and approximate the variance of the statistically distributed variables) X_k are chosen. These are then transformed by the nonlinear process model. A predicted state $\hat{x}_k^-$ is calculated from the transformed sigma points as a weighted mean. Also the new covariance matrix root S_k^- is predicted. Afterwards new sigma points are generated to incorporate the potential process noise and a predicted measurement $\hat{y}_k^-$ is calculated from the measurements generated by these sigma points:

$$X_{k-1} = [\hat{x}_{k-1},\ \eta S_{k-1} + \hat{x}_{k-1},\ -\eta S_{k-1} + \hat{x}_{k-1}] \tag{25}$$

$$X_{k|k-1} = f(X_{k-1}, u_{k-1}) \tag{26}$$

$$\hat{x}_k^- = \sum_{j=0}^{2N} w_j^{(m)} X_{j,k|k-1} \tag{27}$$

$$S_k^- = \text{qr}\left[\sqrt{w_1^{(c)}}(X_{1:2N,k|k-1} - \hat{x}_k^-),\ \sqrt{R_v}\right] \tag{28}$$

$$S_k^- = \text{cholupdate}\left\{S_k^-, X_{0,k|k-1} - \hat{x}_k^-, w_0^{(c)}\right\} \tag{29}$$

$$X_{k|k-1}^* = \left[\hat{x}_k^-,\ \eta S_k^- + \hat{x}_k^-,\ -\eta S_k^- + \hat{x}_k^-\right] \tag{30}$$

$$Y_{k|k-1} = h(X_{k|k-1}^*) \tag{31}$$

$$\hat{y}_k^- = \sum_{j=0}^{2N} w_j^{(m)} Y_{j,k|k-1} \tag{32}$$

In these equations, $\eta = \sqrt{N+\lambda}$ where $\lambda = N(\alpha^2 - 1)$, the weights $w_0^{(m)} = \lambda/(N+\lambda)$, $w_0^{(c)} = \lambda/(N+\lambda) + (1 - \alpha^2 + \beta)$, and $w_j^{(m)} = w_j^{(c)} = 1/(2(N + \lambda))$. All matrix-vector operations in this algorithm are performed column-wise.

Correction. For the calculation of the correction gain K_k at first the covariances from the predicted measurements and the covariance of the transformed sigma points and the generated measurements are calculated to incorporate the measurement noise. Using this information the gain is calculated and the predicted state $\hat{x}_k^-$ and the predicted covariance matrix root S_k^- are updated using the available process measurement y_k:

Table 1. Process Parameters for the Batch Spray Granulation Process

Bed mass (kg)	m_{bed}	10.0
Mass flow of nuclei (kg s^{-1})	M_{nuc}	5.55×10^{-5}
Mass flow of suspension (kg s^{-1})	M_{sus}	1.38×10^{-2}
Solid density (kg m^{-3})	ϱ_s	1000.0
Size of nuclei (m)	ξ_0	0.1×10^{-3}
Simulation time interval (s)	t_{end}	10000.0
Measurement time interval (s)	Δt	50.0
Variance of measurement (m^2)	R_n	10^{-10}
Process noise covariance ($m^{-1}s^{-1}$)	R_v	$10^{-40} I_N$
Design parameter SRUKF	α	0.7

$$S_{y_k}^- = \text{qr}\left[\sqrt{w_1^{(c)}}(Y_{1:2N,k|k-1} - \hat{y}_k^-),\ \sqrt{R_n}\right] \tag{33}$$

$$S_{y_k}^- = \text{cholupdate}\left\{S_{y_k}, Y_{0,k|k-1} - \hat{y}_k^-, w_0^{(c)}\right\} \tag{34}$$

$$P_{x_k y_k} = \sum_{j=0}^{2N} w_j^{(c)} \left[X_{j,k|k-1} - \hat{x}_k^-\right]\left[Y_{j,k|k-1} - \hat{y}_k^-\right]^T \tag{35}$$

$$K_k = (P_{x_k y_k}/S_{y_k}^T)/S_{y_k} \tag{36}$$

$$\hat{x}_k = \hat{x}_k^- + K_k(y_k - \hat{y}_k) \tag{37}$$

$$S_k = \text{cholupdate}\left\{S_k^-, K_k S_{y_k}, -1\right\} \tag{38}$$

In this algorithm $\alpha \in [10^{-4},1)$ is a design parameter that influences the dynamics of the estimator. As it will be pointed out later the choice of α is not arbitrary. The parameter β incorporates some a priori knowledge about the noise distributions, for Gaussian noise $\beta = 2$ is found to be optimal.[26] Specific noise models for v and w can be incorporated quite easily by augmenting the state vector. The covariances of the noise variables need not be constant but can vary in time or can be state-dependent.

The SRUKF has various advantages over the widely used EKF: (1) It does not need analytical derivatives of the model equations, which are often very difficult to obtain, (2) it also does not require a special structure of the model equations, (3) it can be shown that the estimates obtained by the unscented transform are of at least second order (EKF: first order), and in case of Gaussian noise even of at least third-order, (4) the state covariance matrix is guaranteed to be positive definite, and (5) the computational cost of the SRUKF is equivalent to that of the EKF.

Remark: Although we focus in this work on the growth of particles by layering only, other particle phenomena (e.g., agglomeration) can be be handled easily by this scheme without changes to the methodology. This is because of the aforementioned fact that the SRUKF can be applied to arbitrary vector fields and all phenomena can be cast (at least approximately) into the form of Eq. 22.

Some design guidelines

To design a working state estimator as much a priori knowledge about the process should be used as possible, for instance to choose a suitable measurement rate it is of great help to know the dominant time constant of the process. The choice of the initial covariance matrix (which determines the trust in the initial estimate $\hat{x}_0$) is crucial to the performance of the estimator. Too small values lead to small corrections, and therefore, slow down the convergence of the estimate to the process state.

The introduction of additional noise into the estimator can help to stabilize the algorithm, a fact also known from the original Kalman filter, see Ruymgaart and Soong.[29] This is especially true if the measurement is almost noise-free.

The parameter α must be chosen such that the Cholesky downdate of the covariance matrix root in the correction step is always possible. A measurement interval that is too large for the process dynamics can lead to a large correction (e.g., in case of very steep gradients in the state during this time interval), which may result in a downdated covariance matrix that is no longer positive definite. In this case, the algorithm breaks down. One possible solution is to choose a new value of α, another to decrease the time interval of measurements (which need not be equidistant). As it is possible to determine the maximum value of α — given the correction term and the covariance matrix — for which a downdate will be successful, it might be possible to introduce a time-variant parameter α_k, but it is currently not known how the estimator properties are influenced by this.

Simulation Results

To test the SRUKF for both processes the model equations are discretized by a finite volume method using a first-order upwind scheme for the growth term. In every simulation $N = 100$ control volumina are introduced for the discretised property coordinate. This choice provides an acceptable tradeoff between speed of computation and numerical diffusion in the solution of the equations.

The equations are implemented in the MATLAB environment, for the integration the *ode15s* routine is used, a variable order numerical differentiation formula.[30] The estimator equations were rewritten in order to use the time optimized linear algebra methods as often as possible.

The process parameters for the batch granulation process and the continuous granulation process with external classification and particle reflux can be found in Table 1 and Table 2, respectively.

In all simulations the only measurement information available is the average particle size $\tilde{y}_1$ [cf. eq. (17)]. The performance of the estimator is judged by considering the error

$$E(t) = \int_{\xi_0}^{\xi_{\max}} (n(t,\xi) - \hat{n}(t,\xi))^2 \,\mathrm{d}\xi,$$

Table 2. Additional Process Parameters for the Continuous Granulation Process

Screen size upper screen (m)	ξ_u	0.5×10^{-3}
Screen size lower screen (m)	ξ_l	0.4×10^{-3}
Milling diameter (m)	ξ_M	0.35×10^{-3}
Milling diameter (osc.) (m)	ξ_M	0.2×10^{-3}
Measurement time interval (s)	Δt	10.0
Design parameter SRUKF	α	0.6

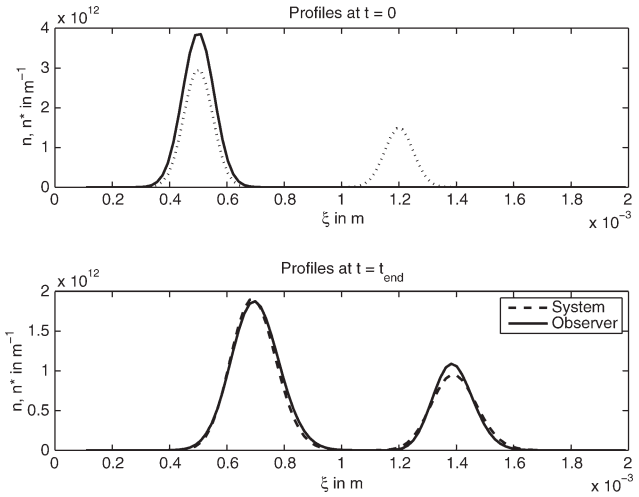

Figure 7. Profiles of the particle size distribution density at $t = t_{end}$ of the plant and the observer.

which is normalized with respect to the initial error $E_0 = E(t = 0)$.

All simulations are perfomed on a standard personal computer (dual core processor with 2.4 GHz and 2 GB RAM), time references always denote wall times as delivered by MATLAB's *tic*/*toc* commands.

Batch granulation process

Three different scenarios were considered to test the designed state estimator:

1. measurement noise,
2. measurement noise and process noise,
3. wrong estimator parameters (robustness test).

Scenario 1. In this scenario normally distributed measurement noise in the order of 10% of the measurement was added to the simulated plant measurement to create a noisy measurement which was then used in the estimation algorithm. As initial condition a bimodal distribution was chosen for the plant. The initial guess provided for the estimator considered only a mono-modal distribution, which is overestimated in magnitude by 30%, see the upper part of Figure 7. This choice leads to a difference in the growth velocity of the estimator model that influences all states of the model. This rather large deviation in the initial distributions is chosen to highlight that the known and unknown modes do not need to overlap in order to be reconstructed, that is, even large initial errors can be corrected. But, it has to be noted that the time necessary to compensate the error depends on the initial deviation.

However, as can be seen in the lower part of Figure 7, the estimation of the particle size distribution is quite good. The known but overestimated mode is reconstructed almost exactly, only a slight deviation in position of the mean and a slighty too large variance can be noticed. The position of the second mode — initially unknown — is estimated with a very small offset, the magnitude of the peak is overestimated as is the variance. The time evolution of the estimation error E/E_0 is depicted in Figure 8. It can be seen that the error decreases almost uniformly over time. The error at the end of the simulation interval can be further decreased by increasing the simulation time or decreasing the time interval of measurements (more measurements, more corrections). In most practical applications, the initial error will be smaller and the convergence will be achieved much faster, which allows a use of this estimatior in an advanced control scheme.

Scenario 2. In addition to Scenario 1 process noise $R_v = 10^{-4}P_0$ was added to the estimator model, for example to incorporate unknown dynamics in the form of small random external disturbances. For the simulations P_0 is calculated by the dyadic product of the differences between model and observer state. To maintain positive definiteness a small multiple of the identity matrix is added. As can be seen in Fig. 9 the error E/E_0 also decreases in time. The decrease appears to be smoother than in Scenario 1 which might be caused by the stabilizing effect of noise on the estimator algorithm.

The estimated profile also corresponds very well to the real density distribution, see Figure 10: The position of the peaks is almost exactly reconstructed, only a deviation in the variance and the magnitude of the second mode can be noticed.

Scenario 3. In practice not all process parameters are known exactly, or errors might occur in the setup of the estimator parameters. For application the estimation algorithm therefore has to possess a certain robustness to parametric errors. In case of the batch granulation process under noisy measurements this robustness is tested by applying a mass flow rate of suspension that is 10% larger than the actually supplied rate. As this parameter is part of the growth rate this error affects all states of the estimator.

In Figure 11 it can be seen that even in this case the estimation error decreases. It can also be seen that at $t = t_{end}$ the error is larger than in the other two scenarios. The estimated profile (Figure 12) shows a larger deviation in the position and the magnitude of the peaks. The variance for both modes is also overestimated.

Because of the difference between the estimator model and the reference process the estimation error will never decrease to zero. The error in the estimator model will always produce predictions that deviate from the reference

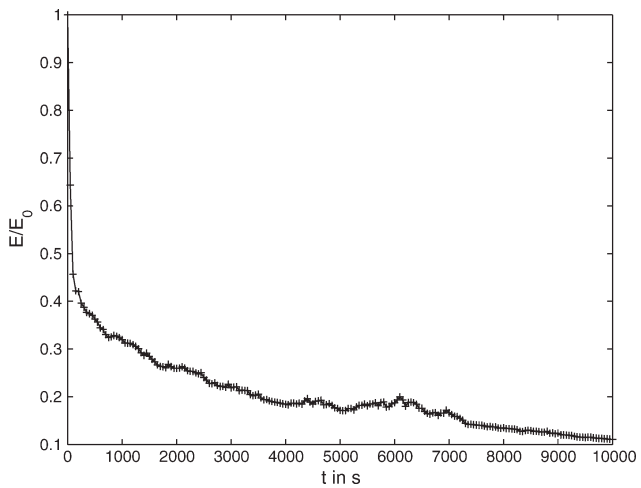

Figure 8. Time evolution of the normalized estimator error E/E_0 in case of noisy measurements.

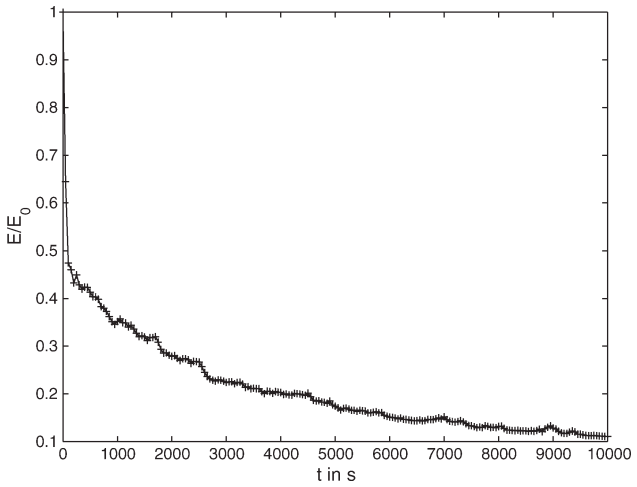

Figure 9. Evolution of the estimator error in case of measurement and process noise.

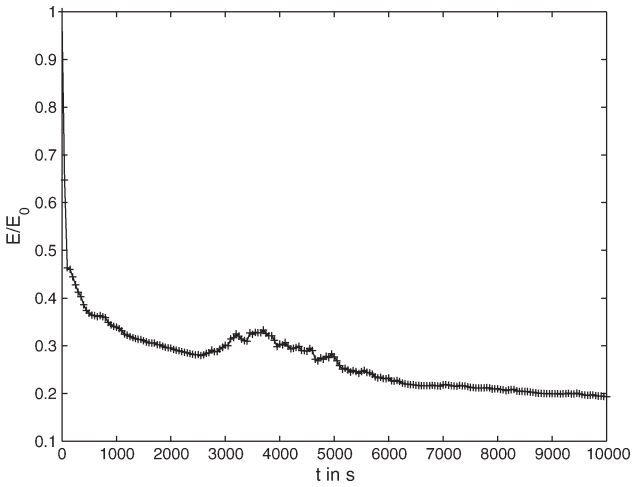

Figure 11. In case of parametric errors the estimator error also decreases.

This decrease is slower than in the other scenarios and tends to a fixed value.

process. These deviations are largely compensated in the update step, but will increase again in the next prediction interval. If the source of the model error is known, one can try to estimate this one as well. In general one will never have a perfect estimator model, and therefore, has to accept a nonzero estimation error.

This result shows that in case of a batch granulation process the estimator is able to compensate up to a certain degree parametric errors, but to get most precise estimates it is necessary to supply precise parameter values.

Continuous granulation with external classification

For each regime of the continuous process the estimator was tested in the following situations:

1. measurement noise,
2. robustness with respect to parameter errors (same dynamic regime),
3. robustness with respect to parameter errors (different dynamic regime),

In the following a leading "1" denotes the set of process parameters that yield a stable steady-state behavior, "2" denotes the set of parameters that lead to an oscillatory behavior. The second number then denotes the situations described above.

In all cases the simulated measurement from the plant model is disturbed in the order of 10% of the measured value to create a noisy measurement for the designed SRUKF. It has to be noted that the same SRUKF was designed and tested for both dynamic regimes.

Scenario 1/1. In this first scenario only measurement noise is taken into account. As an initial condition a uniform particle size distribution with a prespecified mass is chosen

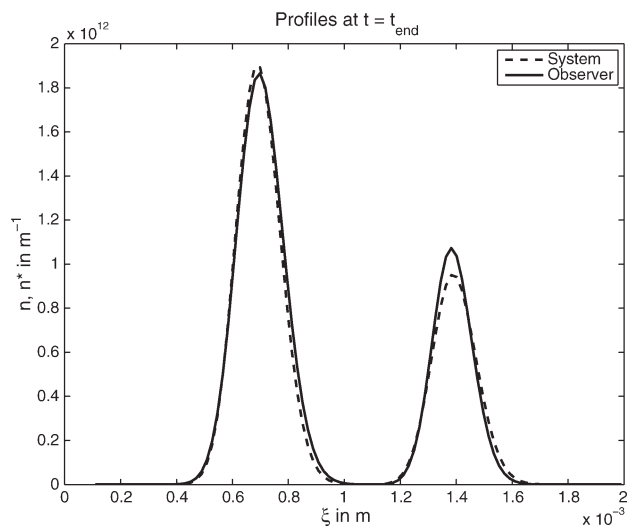

Figure 10. Estimated size distribution density in case of measurement and process noise.

The results are almost identical to Scenario 1.

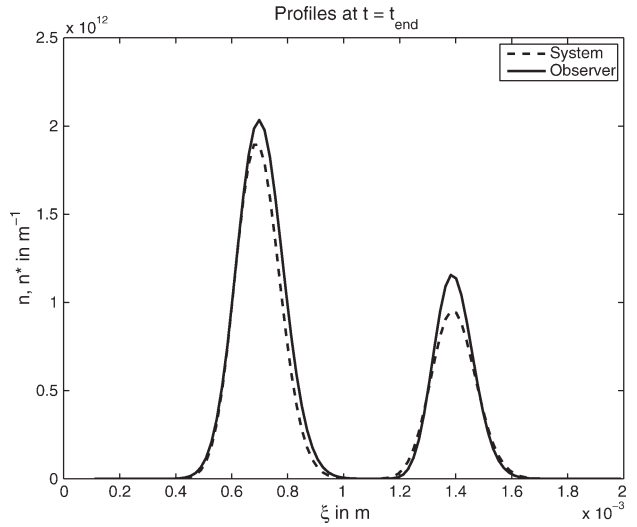

Figure 12. Reconstructed size distribution density in the presence of parametric model errors.

As expected the parametric errors are only compensated up to a certain degree.

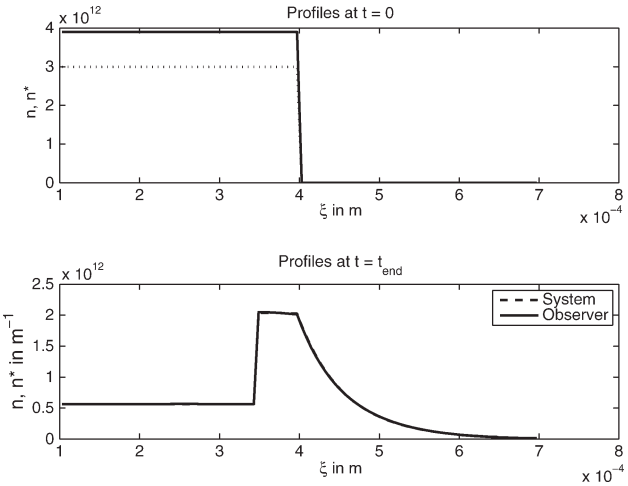

Figure 13. Initial and reconstructed state profiles of process and estimator model for the continuous granulation process (steady-state).

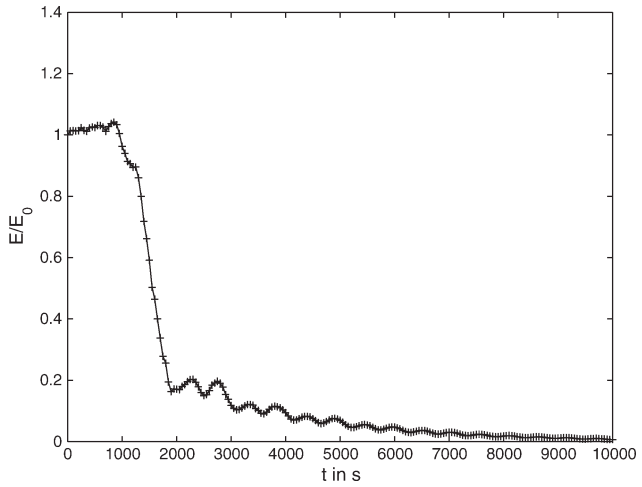

Figure 15. Time evolution of the estimator error for the continuous process under noisy measurements (steady-state).

for the plant model. The estimator model is initialized with a distribution that is off by 30% (upper part of Figure 13). As in case of the batch process this large initial error will slow down the convergence but show that even large errors in the profiles can be corrected. In most practical applications, the initial error will be smaller and the convergence will be achieved much faster.

A characteristic plot of the simulated (noise-free) process measurement, the noisy measurements used in the estimator and the measurements calculated from the estimated states is shown in Figure 14. After a certain time the measurement attains a steady-state value. In the estimator error plot, Figure 15, it can be seen that the error decreases to zero, the size distribution and the estimated distribution are almost indistinguishable, see Figure 13 (lower part).

Scenario 1/2. In this scenario the robustness of the estimator for the continuous process is tested with respect to parametric errors. The diameter ξ_M of the mill that crushes the oversized particles from the first screen is set to a two-and-a-half percent larger value in the estimator than in the model of the process. This influences the particle reflux and through this the growth rate in the estimator model.

In Figure 16 the estimator error for this scenario is plotted. After a short initial period where the error increases, the SRUKF is able to correct the state estimates. The error then decreases showing damped oscillatory behaviour before it reaches a steady-state offset. In Figure 17 which shows the absolute value of the difference between the size distribution and the estimated size distribution it can be seen that the estimator error lies in the interval of the milling diameter error

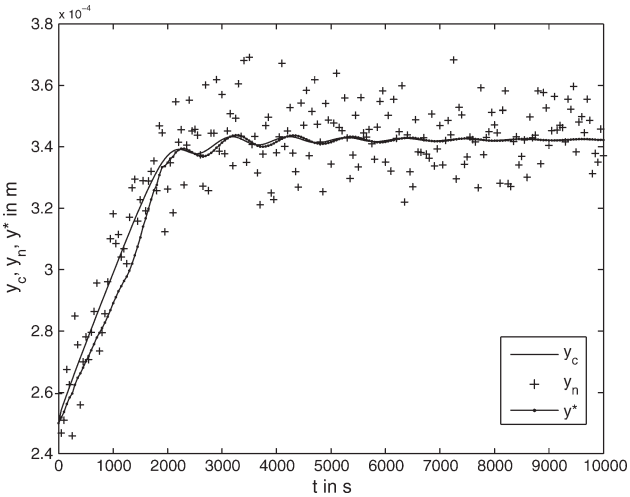

Figure 14. Simulated plant measurement (dashed), noisy measurement (+), and estimated measurement for the continuous process (steady-state regime).

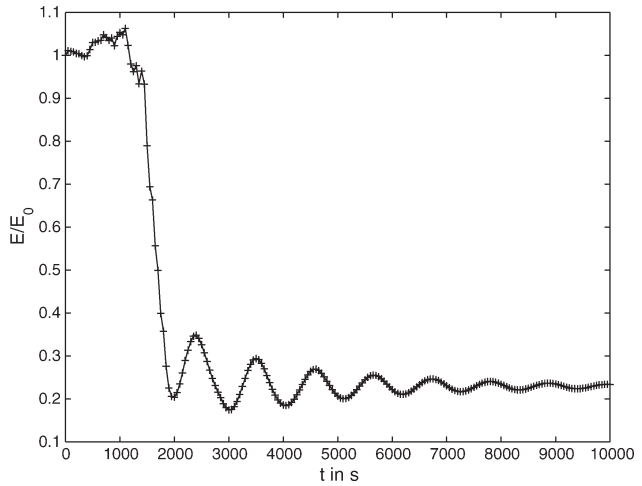

Figure 16. Plot of the estimator error versus time in case of a parametric error in the estimator (same dynamic regime).

After a brief period where the error is larger than the initial one, $E/E_0 > 1$, the error is decreased to a steady-state value.

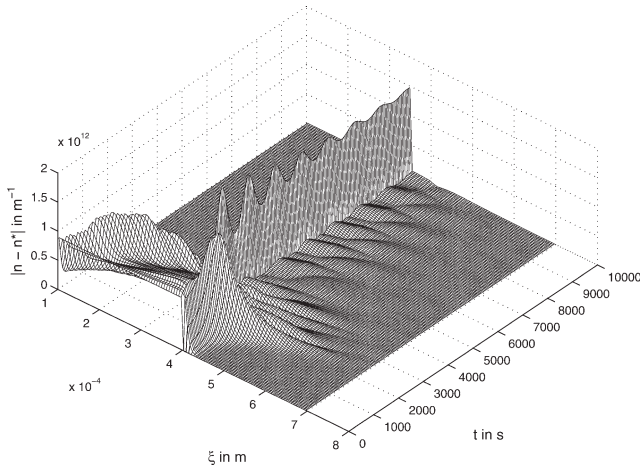

Figure 17. Three-dimensional plot of the absolute difference between size distribution n and estimated distribution $\hat{n}$ for the robustness test.

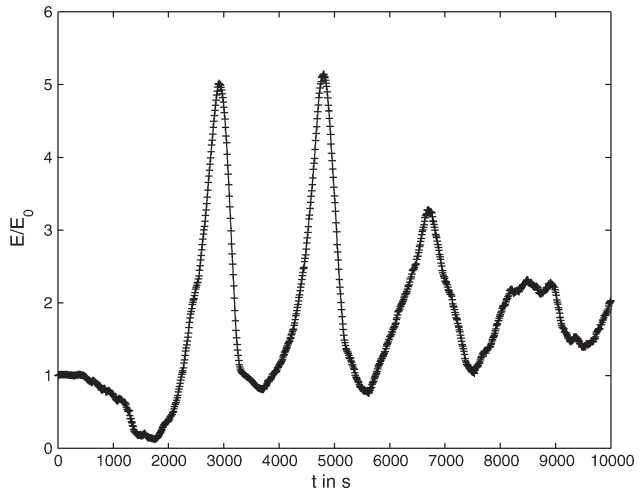

Figure 19. Plot of the estimator error for parametric errors.

The errors are such that the dynamic regimes of process and estimator model are different. As $E/E_0 > 1$ for almost all times the estimation is not successful (steady-state).

and is only slightly corrected. In the profiles one observes a shift of the estimated distribution to higher particle sizes (Figure 18). It can be concluded that the milling diameter has a strong influence on the functionality of the estimator and that error can hardly be compensated.

Scenario 1/3. As a last test the process model is set up for the steady-state regime, whereas the estimator model is set up for the oscillatory regime by an appropriate adjustment of the milling diameters. All other conditions and parameters remain unchanged. As can be seen from the error plot in Figure 19 the estimator is not able to reconstruct the state profile as E/E_0 is greater or equal to one for almost the whole simulation interval. An inspection also shows that values for the size distribution are estimated that are not physically meaningful, for example, negative particle size densities. This is because of the great differences in the dynamic behavior of the two processes, which can not be compensated by the estimator.

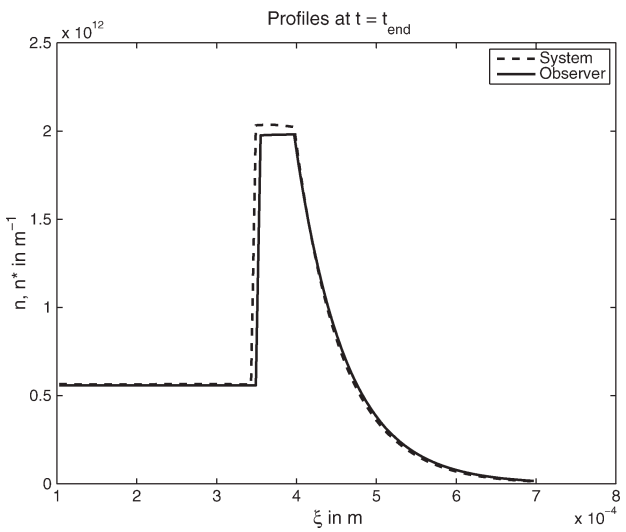

Figure 18. Comparison of real and estimated process profiles under parametric model errors in the same dynamic regime (steady-state).

Scenario 2/1. In this scenario it is tested how the estimator performs in case of an oscillatory process behavior. Therefore, a milling parameter is chosen that leads to sustained oscillations in the particle size distribution density which is shown qualitatively in Figure 6. Here, we used the same initial condition as in the steady-state case, as it provides oscillations with a reasonable amplitude and period. The reconstruction also works for other initial distributions in the process as long as the initial profile of the estimator is close enough to this one.

To fulfill the requirements of the estimation algorithm (see the remark above) the measurement time interval has to be decreased. As in the batch process scenarios a constant time interval is chosen. As can be seen in the plot in Figure 20 the error decreases only very slowly and nonuniformly. The error peaks correspond to the peaks in the size distribution and are due to the fact that the initial error in the profiles of process and estimator model introduces an error in the growth rate that leads to a deviation in the (temporal) position of the peaks. For times where theses peaks do not occur the estimation of the profiles is quite good — only a slight overestimation of the magnitude occurs, see Figure 21. However, the magnitude of the peaks is decreasing so that with a further increase of the number of measurements (and therefore state corrections) the convergence of the error to zero can be accelerated. The price that has to be paid for this is the increase in computation time. With the choices made for this scenario the estimator uses almost eighty percent of the simulation time. A further increase in the number of measurements will also increase this ratio, which will make it difficult to use the scheme in feedback control mechanisms, which also need time to calculate the appropriate control inputs to the process.

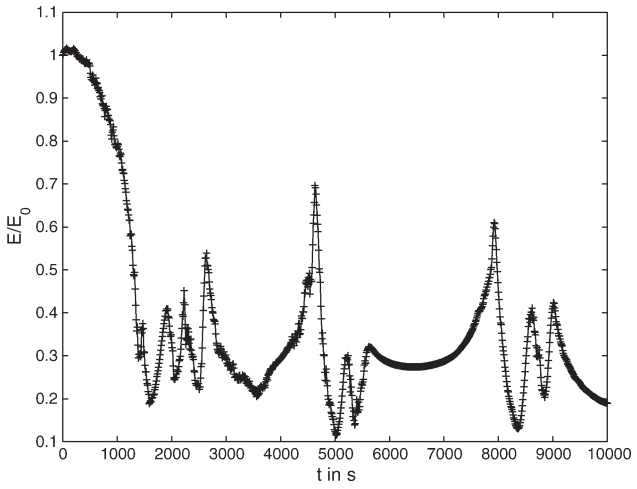

Figure 20. Plot of the estimator error versus time.

The decrease is nonuniform and large peaks appear (osc. regime, constant measurement time interval).

Two possible solutions to this problem are now described briefly: First is the use of parallel implementation of the estimator algorithm on a network of computers in order to propagate the sigma points in the prediction step (the most time-consuming task). This is possible because the propagation in time of one sigma point is independent of the propagation of all other sigma points. As was demonstrated in Mangold et al.[14] this reduces the wall clock time significantly.

Another possible solution is the aforementioned use of a priori knowledge on the process. In this case, the time interval of measurements is chosen such that the dynamics of the process is taken into consideration: During times where the changes are quite slow a larger measurement interval is chosen, at times where steep gradients appear the number of measurements is increased significantly. This approach is demonstrated in Figure 22. The time intervals where the number of measurements has to be increased are determined from process simulations.

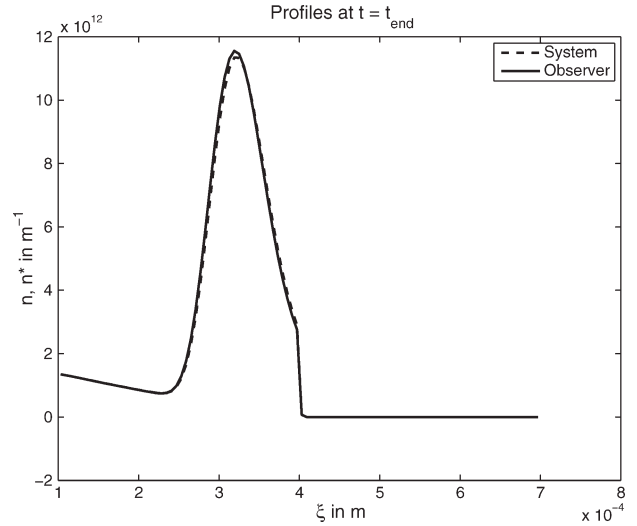

Figure 21. Estimation result of the particle size density distribution for nonpeak times (osc. regime, constant measurement time interval).

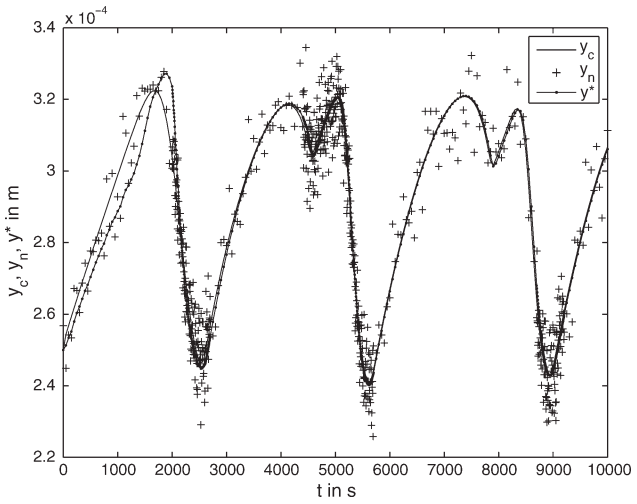

Figure 22. Simulated plant measurement (dashed), noisy measurement (+), and estimated measurement for the continuous process with process-adapted measurement interval (osc. regime).

The estimator error, depicted in Figure 23, shows the positive effect of this adapted measurement intervals, compare Figure 20. Although the qualitative behavior is similar to the case of a constant measurement interval the magnitudes are in general lower and the overall decrease in the error is larger. The errors that correspond to the peaks in the distribution are reduced significantly, see for instance the peak at $t \approx 4500$ *s*. The quality of the estimated profile is as good as in the constant interval case. However, as the total number of measurements is smaller than in the aforementioned case the wall clock time is reduced to about 50% of the simulation time. This provides a better time margin for the use of the estimator in feedback control schemes.

Scenarios 2/2 and 2/3. As a first robustness test an error in the milling diameter of the estimator model is introduced. Both models are still in the oscillatory regime. For the estimation a constant measurement time interval is used.

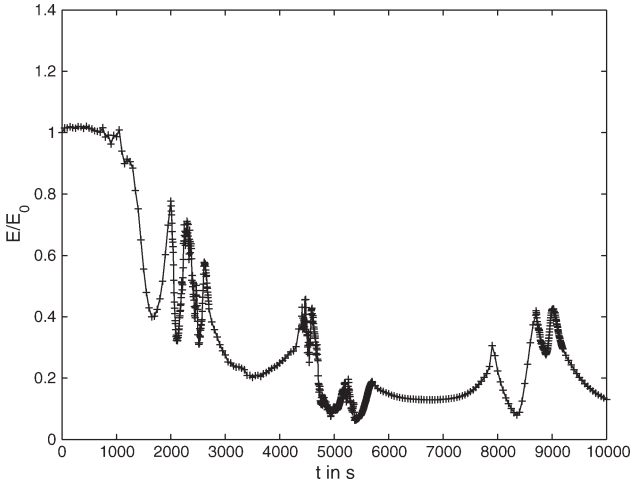

Figure 23. Estimator error evolution for the oscillatory process with dynamic-adapted measurement intervals.

The error decreases nonuniformly with intermediate increases, but a good estimation of the profile is achieved with a slight deviation in position and magnitude of the peaks.

A robustness test for different dynamic regimes of the models shows that the estimator is not able to reconstruct the particle size distribution, that is $E/E_0 > 1$ for almost all times.

These results show that the estimator is only able to compensate parametric model errors up to a certain degree. If a change in the dynamics occurs due to the error the state estimation is not successful.

Summary and Outlook

In this work, we presented an application of model-based measurement for the determination of particle size distributions to two practically relevant granulation processes. We have shown that in principle every (normalized) moment of the size distribution density satisfies the conditions of structural observability, which is necessary for the use in such a measurement scheme. Afterwards SRUKFs were designed and implemented that allowed the dynamic estimation of the particle size distribution density from noisy process measurements. Simulation results show that the scheme is usable for this type of process and different regimes of dynamic behavior, even in the presence of large measurement noise, process noise or parametric model errors. It was also shown that the state estimation is only successful if the parametric model errors do not induce a qualitative change in the dynamics of the processes.

Next will be the validation of these results by using measurement data from experiments, and the comparison of the performance of this estimator with other state observation schemes, for example, a steady-state observer for the continuous process in its steady-state regime. To increase the speed of computation of the estimator algorithm the use of specialised numerical methods will be investigated that provide a comparable accuracy in the solution with a smaller number of grid nodes. Ultimately, the estimated state profiles will be used in a feedback control system to shape the particle size distribution density directly.

Acknowledgments

The authors gratefully acknowledge the funding of this work by the German Federal Ministry of Science and Education (BMBF) as part of the InnoProfile project NaWiTec. The first author acknowledges the support of Dietrich Flockerzi (MPI Magdeburg) in verifying the condition of non-contraction of the process models.

Literature Cited

1. Kail N, Marquardt W, Briesen H. Estimation of particle size distributions from focused beam reflectance measurements based on an optical model. *Chem Eng Sci*. 2009;64:984–1000.
2. Hulburt HM, Katz S. Some problems in particle technology: a statistical mechanical formulation. *Chem Eng Sci*. 1964:19.
3. Ramkrishna D. *Population Balances: Theory and Application to Particulate Systems in Engineering*. New York: Academic Press, 2000.
4. Kalman RE. A new approach to linear filtering and prediction problems. *(Series D)*Trans ASME–J Basic Eng. 1960;82:35–45.
5. Luenberger DG. An introduction to observers. *IEEE Trans Automatic Control*. 1971;16:596–602.
6. Kou SR, Elliot DL, Tarn TJ. Observability of nonlinear systems. *Inform Contr*. 1973;22:89–99.
7. Hermann R, Krener A. Nonlinear controllability and observability. *IEEE Trans Automatic Control*. 1977;20:728–740. Folder A.
8. van der Schaft AJ. Observability and controllability for smooth nonlinear systems. *SIAM J Contr Optimiz*. 1982;20:338–354.
9. Bestle D, Zeitz M. Canonical form observer design for non-linear timevariable systems. *Int J Control*. 1983;38:419–431.
10. Krener AJ, Respondek W. Nonlinear observers with linerizable error dynamics. *SIAM J Contr Optimiz*. 1985;23:197–216.
11. Zeitz M. Nichtlineare Beobachter fr chemische Reaktoren, (Habilitation thesis). Dusseldorf, Germany: VDI-Verlag, 1977.
12. Aguilar-López R, Maya-Yescas R. State estimation for nonlinear systems under model uncertainties: a class of sliding-mode observers. *J Process Control*. 2005;15:363–370.
13. Bastin G, Dochain D. *On-line estimation and adaptive control of bioreactors*. Amsterdam: Elsevier, 1990.
14. Mangold M, Bück A, Schenkendorf R, Steyer C, Voigt A, Sundmacher K. Two state estimators for the barium sulfate precipitation in a semi-batch reactor. *Chem Eng Sci*. 2009;64.
15. Wiberg DM. *State Space and Linear Systems*. New York: McGraw-Hill Book Company (Schaum's Outline), 1971.
16. Nijmeijer H, van der Schaft AJ. *Nonlinear Dynamical Control Systems*. New York: Springer-Verlag, 1991.
17. Isidori A. *Nonlinear Control Systems*; 2nd ed. Berlin and New York: Springer-Verlag, 1989.
18. Reinschke KJ. *Multivariable Control: A Graph-Theoretic Approach*. Akademie-Verlag: Berlin, 1988.
19. Wend H-D. Strukturelle Analyse linearer Regelungssysteme: Verfahren zur Untersuchung grundlegender Systemeigenschaften auf der Basis parameterunabhängiger Modelle, (Habilitation thesis). Oldenbourg, 1993.
20. Heinrich S, Peglow M, Ihlow M, Mörl L. Particle population modeling in fluidized bed-spray granulation—analysis of the steady state and unsteady behavior. *Powder Technol*. 2003;130:154–161.
21. Radichkov R, Müller T, Kienle A, Heinrich S, Peglow M, Mörl L. A numerical bifurcation analysis of continuous fluidized bed spray granulation with external product classification. *Chem Eng Process*. 2006;45:826–837.
22. Ennis BJ, Tardos G, Pfeffer R. A microlevel-based characterization of granulation phenomena. *Powder Technol*. 1991;65:257–272. A Special Volume Devoted to the Second Symposium on Advances in Particulate Technology.
23. Mörl L, Heinrich S, Peglow M. *Granulation*. In: Salman AD, Hounslow MJ, Seville JPK, editors. Chapter Fluidized Bed Spray Granulation, Amsterdam: Elsevier B. V., 2007;21–188.
24. Evans LC. *Partial Differential Equations*. Providence, RI: American Mathematical Society, 2002.
25. Sorenson HW. Least-squares estimation: from Gauss to Kalman. *IEEE Spectrum*. 1970;7:63–68.
26. Julier S, Uhlmann JK, Durrant-Whyte HF. A new method for the nonlinear transformation of means and covariances in filters and estimators. *IEEE Trans Automatic Control*. 2000;45:477–482.
27. Julier SJ, Uhlmann JK. Unscented filtering and nonlinear estimation. *Proc IEEE*. 2004;92:401–422.
28. van der Merwe R, Wan EA. The square-root unscented Kalman filter for state and parameter estimation. *International Conference on Acoustics, Speech, and Signal Processing, Salt Lake City, Utah*, 2001.
29. Ruymgaart PA, Soong TT. *Mathematics of Kalman-Bucy Filtering*. Berlin: Springer-Verlag, 1988.
30. Shampine LF, Reichelt MW. The MATLAB ODE Suite. *SIAM J Sci Comput*. 1997;18:1–22.

Manuscript received July 20, 2009, and revision received May 3, 2010.